ANNALS OF MEDICINE
2026, VOL. 58, NO. 1, 2634444
https://doi.org/10.1080/07853890.2026.2634444

RESEARCH ARTICLE

OPEN ACCESS Check for updates

Integrated machine learning risk model for predicting radiation pneumonitis in lung cancer patients with interstitial lung disease

Haozheng Lu[#], Aimin Jiang[#], Zhaoqi Yuan and Dawei Chen

Shandong Provincial Key Laboratory of Precision Oncology, Shandong Cancer Hospital and Institute, Shandong First Medical University and Shandong Academy of Medical Sciences, Jinan, Shandong, China

ABSTRACT

Background: Radiation pneumonitis (RP) is a serious complication in lung cancer patients with pre-existing interstitial lung disease (ILD) undergoing radiotherapy. Accurate risk stratification is crucial for individualized management. But predictive models integrating multimodal data are lacking. This study aimed to develop a novel machine learning-based nomogram integrating clinical, dosimetric, and inflammatory predictors for RP risk assessment in this high-risk population.

Methods: This retrospective study of 424 ILD patients collected clinical, dosimetric, and inflammatory data. Machine learning algorithms created composite dosimetric (*D* score) and inflammatory (Inflamm score) scores. A multivariable logistic regression nomogram was built incorporating these scores with clinical risk factors. Model performance was assessed using area under the curve (AUC), calibration curve, and decision curve analysis (DCA).

Results: RP occurred in 200 (47%) patients. Independent risk factors included higher performance status, Charlson comorbidity index (CCI), usual interstitial pneumonia (UIP) pattern, immunotherapy, concurrent chemoradiotherapy, more radiation sessions, and lower lung volume. The *D* score and Inflamm score were both independent predictors. The integrated nomogram (AUC = 0.929) showed excellent discrimination, significantly outperforming the clinical model (AUC = 0.86), *D* score (AUC = 0.758) (both $p<0.001$), and Inflamm score (AUC = 0.910, $p=0.168$). Calibration curve and DCA confirmed its strong calibration ability and clinical utility to identify high-risk patients early.

Conclusion: The integrated nomogram combining clinical, dosimetric, and inflammatory predictors enables accurate, individualized RP risk assessment in lung cancer patients with ILD. It can guide adjustments to individualized radiotherapy plans or preventive interventions, supporting better patient selection, treatment decisions, and proactive follow-up.

ARTICLE HISTORY
Received 21 August 2025
Accepted 7 February 2026

KEYWORDS
Interstitial lung disease; lung cancer; machine learning; radiation pneumonitis; risk prediction

Introduction

Radiotherapy remains a cornerstone in the management of lung cancer. However, the unique radiosensitivity of alveolar tissue renders patients susceptible to radiation-induced toxicities [1]. Complications such as radiation pneumonitis (RP) limit the safe application of radiotherapy in broader populations [2]. Interstitial lung disease (ILD), characterised by diffuse parenchymal inflammation and fibrosis [3], is both a risk factor for lung cancer and a common comorbidity in lung cancer patients [4]. Notably, pre-existing ILD markedly elevates the risk of RP as well as immune checkpoint inhibitor pneumonitis (CIP) [5], and ILD is recognised as a critical determinant of adverse pulmonary outcomes following radiotherapy [6]. Despite these established risks, there remains an urgent need to develop reliable individualized risk stratification tools to accurately predict the likelihood of RP development in patients.

CONTACT Dawei Chen dave0505@yeah.net Shandong Provincial Key Laboratory of Precision Oncology, Shandong Cancer Hospital and Institute, Shandong First Medical University and Shandong Academy of Medical Sciences, Jinan, Shandong, China, No. 440 Jiyan Road, 250117, Jinan, Shandong Province, P. R. China.
[#]These authors have contributed equally to this work and share first authorship.
Supplemental data for this article can be accessed online at https://doi.org/10.1080/07853890.2026.2634444.

Most existing models are limited to small-sample cohort studies from single institutions and rely solely on isolated predictors (dosimetric or hematological parameters), making it difficult to achieve individualized and precise prediction of RP [7]. Moreover, integration of molecular features and modern machine-learning (ML) representations remains sparse, despite emerging evidence from deep-learning–based biomarker discovery in lung cancer (e.g. miRNA signatures) that such signals may enhance risk stratification–signals that are typically absent from current RP models [8]. Collectively, these limitations contribute to miscalibration and poor transportability when models are applied outside their derivation settings. Building on these insights, we explicitly incorporate multimodal data and explore ML-enabled fusion of clinical, dosimetric, and inflammatory markers, aligning with emerging evidence that molecular signatures extracted *via* deep learning can enhance risk stratification. ML algorithms are well suited for integrating multimodal data [9] and modelling the multifactorial risk architecture of RP, capturing individual heterogeneity that traditional single-factor models may overlook and thereby improving predictive performance [10]. Despite the critical need, there are currently no validated models capable of integrating clinical features, dose parameters, and inflammatory biomarker information to predict RP in this high-risk population, resulting in suboptimal risk stratification in clinical practice.

This study aims to develop and optimize an integrated predictive model for RP risk in lung cancer patients with comorbid ILD. The model synthesizes clinical indicators, dosimetric parameters, and inflammatory biomarkers. By establishing a comprehensive composite scoring system and a user-friendly nomogram, individualized risk assessment can be achieved. Ultimately, this tool is intended to improve treatment outcomes and optimize clinical decision-making for this high-risk population.

Materials and methods

Study design and patient population

This retrospective cohort study included patients with histologically confirmed lung cancer and pre-existing ILD who received radiotherapy at Shandong Cancer Hospital between September 2020 and September 2024. The inclusion criteria were as follows: (1) Newly diagnosed lung cancer cases confirmed by pathological examination; (2) radiographic evidence of ILD prior to radiotherapy; (3) availability of imaging data before and after radiotherapy; and (4) complete clinical and dosimetric information. The exclusion criteria were as follows: (1) incomplete clinical or dosimetric data; (2) absence of imaging evidence at the time of RP diagnosis; or (3) a history of prior thoracic radiotherapy. For laboratory variables, single imputation using the mean value was performed if the proportion of missing data was 1%; otherwise, the variable was excluded from the analysis. The details of missing data are presented in Supplementary Table 1. The study protocol was reviewed and approved by the Ethics Committee of Shandong Cancer Hospital and Institute (approval number: SDTHEC 202501010) and conducted in accordance with the Declaration of Helsinki and relevant institutional guidelines. As this is a retrospective analysis, the Ethics Committee of the Shandong Cancer Hospital and Institute waived the requirement for individual patient informed consent.

The definition of RP

RP is defined as sterile parenchymal lung inflammation occurring weeks to months after thoracic radiotherapy [11]. After excluding infectious etiologies according to clinical guidelines [12], the radiotherapy isodose lines are superimposed onto CT images to assess the spatial concordance between lung lesions and the radiation field, as well as the extent of involvement. If the lesions are predominantly distributed within the high-dose irradiation area, typically presenting as unilaterally located with relatively well-defined borders, they are classified as suggestive of radiation pneumonitis. Sputum culture or bronchoscopy may be performed when necessary to rule out infection. Severity grading is mostly based on Common Terminology Criteria for Adverse Events (CTCAE, version 5.0) [13], and treatment plans are formulated accordingly. When differentiating from immune checkpoint inhibitor-related pneumonitis, attention should be paid to whether the lesions conform to the radiation field, the temporal relationship with drug

administration, and differences in imaging patterns. Checkpoint inhibitor pneumonitis often presents with bilateral or multifocal distribution and does not conform to the irradiation field [14].

Data collection and covariates

This retrospective study extracted demographic, clinicopathological, and imaging data from the hospital's electronic medical record system, laboratory variables from the laboratory information system, and imaging data from the picture archiving and communication system. The data included age, gender, smoking history, performance status (PS), comorbidities (assessed *via* Charlson Comorbidity Index [CCI]), ILD severity and subtype, TNM stage, tumour characteristics, and treatment modalities (immunotherapy, chemotherapy, radiotherapy technique, and number of fractions). Dosimetric parameters were collected from our treatment plan system (Eclipse, Varian Medical Systems, USA). Baseline laboratory data, including complete blood counts and serum albumin, were collected within four weeks prior to the initiation of radiotherapy. Inflammatory and nutritional parameters derived from these laboratory tests, such as the monocyte-to-lymphocyte ratio (MLR), neutrophil-to-lymphocyte ratio (NLR), platelet-to-lymphocyte ratio (PLR), systemic immune-inflammation index (SII), and prognostic nutritional index (PNI), were calculated for subsequent analysis [15–18].

Classification of ILD

The diagnosis and severity of ILD were determined by multidisciplinary evaluation of high-resolution computed tomography (HRCT) and classified according to established criteria. Interstitial lung abnormalities (ILAs) were defined as nondependent parenchymal abnormalities—including ground-glass or reticular abnormalities, architectural distortion, traction bronchiectasis/bronchiolectasis, honeycombing, or nonemphysematous cysts—involving ≥5% of any lung zone; focal or unilateral changes, or abnormalities involving <5% of any zone, were deemed indeterminate [19,20]. The lung parenchyma was divided into six zones (upper, middle, and lower for each lung). For CT scans acquired within 6 months prior to radiotherapy (axial slice thickness 1–5 mm), two thoracic radiologists independently scored, using a standardized atlas, the visual extent of ILA in each zone as 0 (0%), 1 (5 to <25%), 2 (25 to <50%), or 3 (≥50%) [21]. All CT scans were independently reviewed by two primary readers (H.Z.L. and A.M.J.). Discrepancies between the two readers were resolved by consensus with a third senior reader (D.W.C.) serving as an adjudicator. The highest zone score was used as the primary severity grade (None = 0; Mild = 1; Moderate = 2; Severe = 3). If fibrotic features (traction bronchiectasis/bronchiolectasis or honeycombing) were present, the severity grade was escalated by one level, capped at Severe [21]. Consistent with the 2022 clinical practice guideline update from the American Thoracic Society, European Respiratory Society, Japanese Respiratory Society, and Latin American Thoracic Association, CT patterns were classified as usual interstitial pneumonia (UIP), probable UIP, indeterminate for UIP, or alternative diagnosis [22]. For analytic purposes, because some categories contained few patients, and previous studies have combined the 'indeterminate for UIP' and 'alternative diagnosis' categories into a single group [23], we collapsed the patterns into three groups—UIP, probable UIP, and indeterminate for UIP/alternative diagnosis (Supplementary Figure 1)—to improve statistical power and model stability. One patient from each group was randomly selected for illustration. All image reviews were performed with readers blinded to the subsequent occurrence of RP.

Dosimetric and inflammatory parameter selection

All relevant dosimetric parameters—including clinical target volume (CTV), lung volume, mean lung dose (MLD), mean heart dose (MHD), and dose volume histogram (DVH, e.g. V20, V30)—as well as baseline hematological and inflammatory indices, were initially included in the analysis. Collinearity among candidate variables was assessed using Spearman's rank correlation coefficients and visualized by correlation heatmaps. Feature selection for both dosimetric and inflammatory predictors was conducted using three ML approaches implemented in R software (version 4.4.2): least absolute shrinkage and selection operator (LASSO) regression (glmnet package), random forest (RF, randomForest package), and extreme gradient boosting (XGBoost, xgboost package). For LASSO, a binomial model ($\alpha = 1$) was fitted and the

optimal penalty parameter lambda was determined *via* 10-fold cross-validation (for the dosimetric set, λ_1se = 0.062736; for the hematologic and inflammatory set, λ_1se = 0.027646). Predictors with non-zero coefficients at the selected λ were retained. Random-forest models were trained with ntree = 500 (other hyperparameters followed package defaults for classification), and variable importance was summarized by mean decrease in accuracy using out-of-bag permutation. XGBoost used a learning rate (eta) = 0.01, max_depth = 4, subsample = 0.8, and colsample_bytree = 0.8; the number of boosting iterations (nrounds) was selected by 10-fold cross-validation with early stopping (10 rounds) from an upper bound of 1000, and the final model used the iteration achieving the highest mean test AUC. Key predictors for radiation pneumonitis (RP) were then identified by intersecting the top-ranked features across the three algorithms (RF importance and XGBoost gain) with the non-zero LASSO coefficients; only variables present in the intersection were retained for subsequent model development.

Development of risk scores and prediction models

Associations between candidate variables and the occurrence of any-grade RP were evaluated using univariate and multivariate logistic regression analyses. Univariate logistic regression was used to screen candidate variables. Variables with $p < 0.05$ were entered into the multivariable logistic regression as candidate predictors without automated stepwise selection, and independent predictors identified in the multivariate analysis were used to establish the basic clinical prediction model. Selected dosimetric and inflammatory variables were each combined into composite risk scores (the *D* score and Inflamm score, respectively), by assigning weights based on logistic regression coefficients and applying *Z* score standardization. A comprehensive model was then developed, integrating independent clinical variables with the *D* score and Inflamm score to improve predictive performance. For individualized RP risk estimation, a nomogram based on the final integrated model was constructed using the rms package in R.

Model evaluation

The predictive performance of each model was primarily assessed using receiver operating characteristic (ROC) curve analysis, with the area under the curve (AUC) calculated to quantify discrimination. ROC curves and AUC values were generated using the pROC package in R. Differences in AUCs between models were compared using DeLong's test. Model calibration was evaluated by calibration plots (rms package) and the Hosmer–Lemeshow goodness-of-fit test. Clinical utility and net benefit were assessed *via* decision curve analysis (DCA) using the rmda or stdca package in R, with interpretation of threshold probabilities at which the model offers superior clinical benefit compared to treat-all or treat-none strategies. Additional subgroup analyses were performed according to clinical characteristics (e.g. radiotherapy technique, ILD subtype) to assess the robustness and generalization of the prediction models.

Statistical analysis

All statistical analyses were performed using R software (version 4.4.2). Continuous variables were summarized as mean ± standard deviation or median and interquartile range (IQR), and compared using the Student's *t* test or Mann–Whitney *U* test as appropriate. Categorical variables were presented as frequencies and percentages, and compared using the chi-square test or Fisher's exact test. Logistic regression was used for univariate and multivariate analyses of risk factors for RP. All statistical tests were two-sided, and a *P* value < 0.05 was considered statistically significant.

Results

Baseline characteristics

As shown in Figure 1, a total of 424 lung cancer patients with pre-existing ILD were included in this analysis, comprising 200 who developed RP and 224 who did not. The median age was similar between groups, and both were predominantly male. Compared to the non-RP group, patients with RP had higher

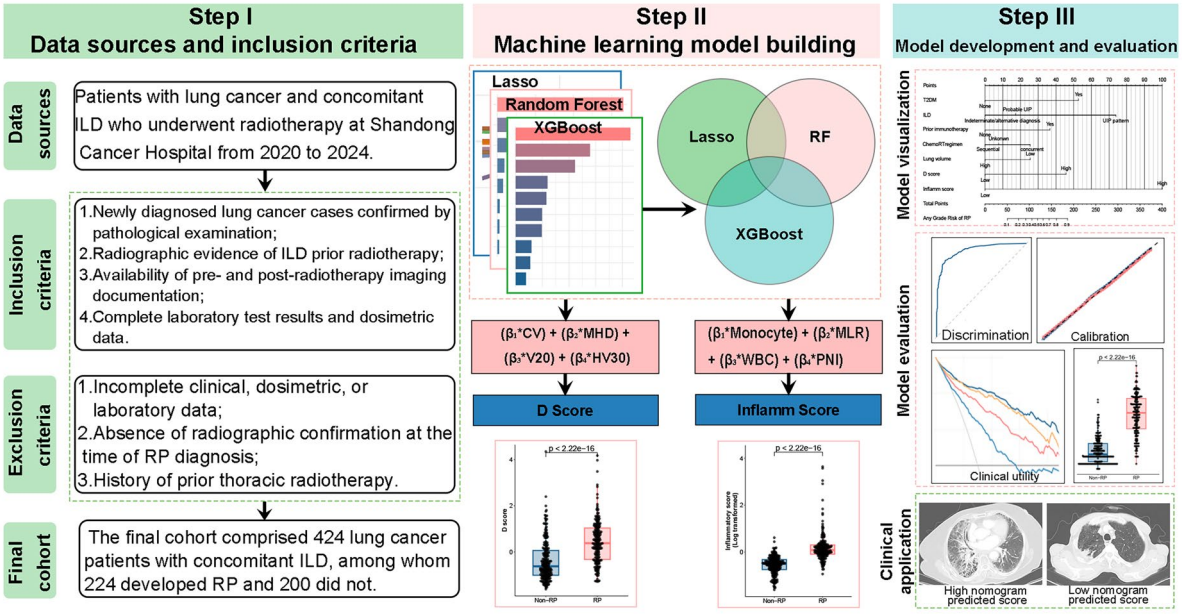

Figure 1. Data filtering and machine learning framework construction. ILD, interstitial lung disease; Lasso, least absolute shrinkage and selection operator; RF, random forest; XGBoost, Xtreme gradient boosting.

CCI scores and were more likely to have type 2 diabetes mellitus (T2DM, 37.5% vs. 7.6%). RP patients also showed greater ILD severity (91% vs. 37.9%) and a higher prevalence of the UIP pattern (23% vs. 4.5%). Patients in the RP group were more likely to have advanced clinical stage (III–IV), higher T (T3–4) and N (N1–3) stages, and poorer performance status (PS 0–1: 30.5% vs. 50%). No significant differences were observed in tumor location, histological subtype, or driver gene alterations. As for treatment, RP patients more frequently received immunotherapy (56% vs. 20.5%), concurrent chemoradiotherapy (44.5% vs. 18.3%), intensity-modulated radiotherapy (IMRT, 90% vs. 71.9%), and ≥28 radiotherapy fractions (65% vs. 42.9%), but were less likely to receive stereotactic body radiotherapy (SBRT, 8% vs. 22.8%). RP patients also had lower lung volumes. Detailed baseline characteristics are summarized in Table 1.

Clinical predictors of RP

Univariate analysis identified low smoking score, higher PS (2), higher CCI, UIP pattern, advanced TNM stage (III–IV), received immunotherapy, concurrent chemoradiotherapy, IMRT technique, number of radiation sessions (≥28), and lower lung volume as significant risk factors for RP (all $p < 0.05$; Supplementary Table 2). In multivariate analysis, higher PS (odds ratio [OR] = 1.74, 95% confidence interval [CI]: 1.03–2.95; $p = 0.039$), higher CCI (OR = 2.49, 95% CI: 0.10–7.69; $p = 0.032$), UIP pattern (OR = 6.11, 95% CI: 2.47–15.13; $p < 0.001$), receive immunotherapy (OR = 4.15, 95% CI: 2.42–7.12; $p < 0.001$), concurrent chemoradiotherapy (OR = 3.13, 95% CI: 1.75–5.56; $p < 0.001$), number of radiation sessions ≥ 28 (OR = 2.13, 95% CI: 1.21–3.75; $p = 0.009$), and lower lung volume (OR = 2.33, 95% CI: 1.38–3.92; $p = 0.002$) were identified as independent risk factors of RP in lung cancer patients with pre-existing ILD (Supplementary Table 2). A multivariable logistic regression model (basic clinical model) incorporating these factors demonstrated strong predictive performance for RP risk, with an area under the curve (AUC) of 0.86 (95% CI: 0.825–0.895; Supplementary Figure 2).

Dosimetric predictors and development of the D score

Baseline dosimetric characteristics are summarized in Supplementary Table 3. Patients who developed RP exhibited significantly higher CTV, MLD, MHD, both lung V20 (BV20), and heart V30 (HV30). Due to strong correlations among these dosimetric parameters (Supplementary Figure 3A). Through LASSO regression, RF, and XGBoost (Figure 2A–E and Supplementary Figure 3B) we identified CTV-to-lung volume ratio (CV),

Table 1. Baseline demographic and clinical characteristics.

Variables	Non-RP ($N=224$)	RP ($N=200$)	P value
Age			0.207
<65	94 (42%)	71 (35.5%)	
≥65	130 (58%)	129 (64.5%)	
Gender			0.109
Female	52 (23.2%)	33 (16.5%)	
Male	172 (76.8%)	167 (83.5%)	
Smoke score			0.001
High	132 (58.9%)	85 (42.5%)	
Low	92 (41.1%)	115 (57.5%)	
BMI group			0.519
Normal	112 (50%)	89 (44.5%)	
Overweight	97 (43.3%)	97 (48.5%)	
Underweight	15 (6.7%)	14 (7%)	
ECGO PS			<0.001
0–1	112 (50%)	61 (30.5%)	
2	112 (50%)	139 (69.5%)	
CCI			0.009
High	197 (87.9%)	191 (95.5%)	
Low	27 (12.1%)	9 (4.5%)	
Hypertension			0.117
None	177 (79%)	144 (72%)	
Yes	47 (21%)	56 (28%)	
T2DM			<0.001
None	207 (92.4%)	125 (62.5%)	
Yes	17 (7.6%)	75 (37.5%)	
Arteriosclerosis			0.092
None	176 (78.6%)	142 (71%)	
Yes	48 (21.4%)	58 (29%)	
COPD			0.171
None	216 (96.4%)	186 (93%)	
Yes	8 (3.6%)	14 (7%)	
ILD score			<0.001
Low	29 (12.9%)	0 (0%)	
Moderate	110 (49.1%)	18 (9%)	
Severe	85 (37.9%)	182 (91%)	
ILD			<0.001
Probable UIP pattern	193 (86.2%)	145 (72.5%)	
Indeterminate and alternative diagnosis	21 (9.4%)	9 (4.5%)	
UIP pattern	10 (4.5%)	46 (23%)	
Stage			<0.001
I–II	58 (25.9%)	25 (12.5%)	
III–IV	166 (74.1%)	175 (87.5%)	
T stage			0.007
T1–2	142 (63.4%)	100 (50%)	
T3–4	82 (36.6%)	100 (50%)	
N stage			<0.001
*N*0	68 (30.4%)	26 (13%)	
*N*1–3	156 (69.6%)	174 (87%)	
M stage			0.169
*M*0	157 (70.1%)	153 (76.5%)	
*M*1	67 (29.9%)	47 (23.5%)	
Cancer location			0.738
Both lungs	5 (2.2%)	3 (1.5%)	
Left lung	97 (43.3%)	82 (41%)	
Right lung	122 (54.5%)	115 (57.5%)	
Lung cancer subtypes			1.000
NSCLC	167 (74.6%)	149 (74.5%)	
SCLC	57 (25.4%)	51 (25.5%)	
Driver gene alterations			0.793
None	188 (83.9%)	165 (82.5%)	
Yes	36 (16.1%)	35 (17.5%)	
Surgical history			0.062
None	176 (78.6%)	172 (86%)	
Yes	48 (21.4%)	28 (14%)	
Receive immunotherapy			<0.001
None	178 (79.5%)	88 (44%)	
Yes	46 (20.5%)	112 (56%)	
ChemoRTregimen			0.040
Concurrent	41 (18.3%)	89 (44.5%)	
Sequential	169 (75.4%)	107 (53.5%)	
Unknown	14 (6.2%)	4 (2%)	

(*Continued*)

Table 1. Continued.

Variables	Non-RP ($N=224$)	RP ($N=200$)	P value
Radiation technique			<0.001
IMRT	161 (71.9%)	180 (90%)	
SBRT	51 (22.8%)	16 (8%)	
VMRT	12 (5.4%)	4 (2%)	
Number of radiation sessions			<0.001
<28	128 (57.1%)	70 (35%)	
≥28	96 (42.9%)	130 (65%)	
Lung volume			<0.001
High	131 (58.5%)	81 (40.5%)	
Low	93 (41.5%)	119 (59.5%)	

CCI, Charlson comorbidity index; COPD, chronic obstructive pulmonary disease; ILD, interstitial lung disease; IMRT, intensity modulated radiotherapy; NSCLC, non-small cell lung cancer; PS, performance status; SBRT, stereotactic body radiotherapy; SCLC, small cell lung cancer; T2DM, type 2 diabetes; UIP, usual interstitial pneumonia; VMRT, volumetric modulated radiation therapy.

MHD, BV20, and HV30 as key dosimetric predictors of RP (Figure 2F). Logistic regression coefficients were used to construct a composite dosimetric risk score (D score):

$$\mathrm{D-score} = (\beta_1 \times \mathrm{CV}) + (\beta_2 \times \mathrm{MHD}) + (\beta_3 \times \mathrm{V20}) + (\beta_4 \times \mathrm{HV30})$$

The D score was standardized using Z score normalization (Figure 2G). Patients with RP had significantly higher D scores than those without RP (Figure 2I). Receiver operating characteristic (ROC) analysis demonstrated robust predictive power (AUC = 0.758, 95% CI: 0.713–0.804; Figure 2H), supporting the utility of the D score for RP risk stratification.

Inflammatory predictors and development of the Inflamm score

Baseline hematological and inflammatory characteristics are shown in Supplementary Table 4. Patients with RP had significantly higher monocyte counts, MLR, total leukocyte count, and lower PNI compared with those without RP. Significant multicollinearity among these variables was noted (Supplementary Figure 3C). Through LASSO regression, RF, and XGBoost algorithms (Figure 3A–E and Supplementary Figure 3D), monocyte count, MLR, leukocyte count, and PNI were consistently identified as key inflammatory predictors of RP (Figure 3F). A composite inflammatory score (Inflamm score) was constructed as follows:

$$\mathrm{Inflamm-score} = (\beta_1 \times \mathrm{monocyte\,count}) + (\beta_2 \times \mathrm{MLR}) + (\beta_3 \times \mathrm{leukocyte\,count}) + (\beta_4 \times \mathrm{PNI})$$

The Inflamm score was standardized prior to analysis (Figure 3G). RP patients had significantly higher Inflamm scores (Figure 3I). ROC analysis showed strong discrimination (AUC = 0.910, 95% CI: 0.882–0.938; Figure 3H), indicating that the Inflamm score effectively stratifies RP risk.

Integrated prediction model for RP risk

To further improve predictive accuracy, clinical predictors, D score, and Inflamm score were integrated into a multivariable logistic regression model. Both the D score and Inflamm score remained independent predictors after adjustment for significant clinical covariates (Table 2). Among clinical variables, T2DM (OR = 4.75, 95% CI: 2.21–10.78; $p<0.001$), UIP pattern (OR = 5.49, 95% CI: 1.98–15.19; $p=0.001$), receipt of immunotherapy (OR = 3.35, 95% CI: 1.76–6.35; $p<0.001$), Concurrent chemoradiotherapy (OR = 2.27, 95% CI: 1.16–4.55; $p=0.017$), and lower lung volume (OR = 2.41, 95% CI: 1.28–4.54; $p=0.007$) were identified as independent predictors.

An integrated nomogram was constructed (Figure 4A) and demonstrated excellent discrimination ability (AUC = 0.929, 95% CI: 0.905–0.952; Figure 4B). DeLong's test showed the integrated model significantly outperformed the basic clinical model (AUC increase: 0.069, $p<0.01$), the D score (AUC increase: 0.171, $p<0.01$), and showed a numerically higher, though not statistically significant performance compared to the Inflamm score (AUC increase: 0.019, $p=0.054$; Table 3). Calibration curves indicated good agreement

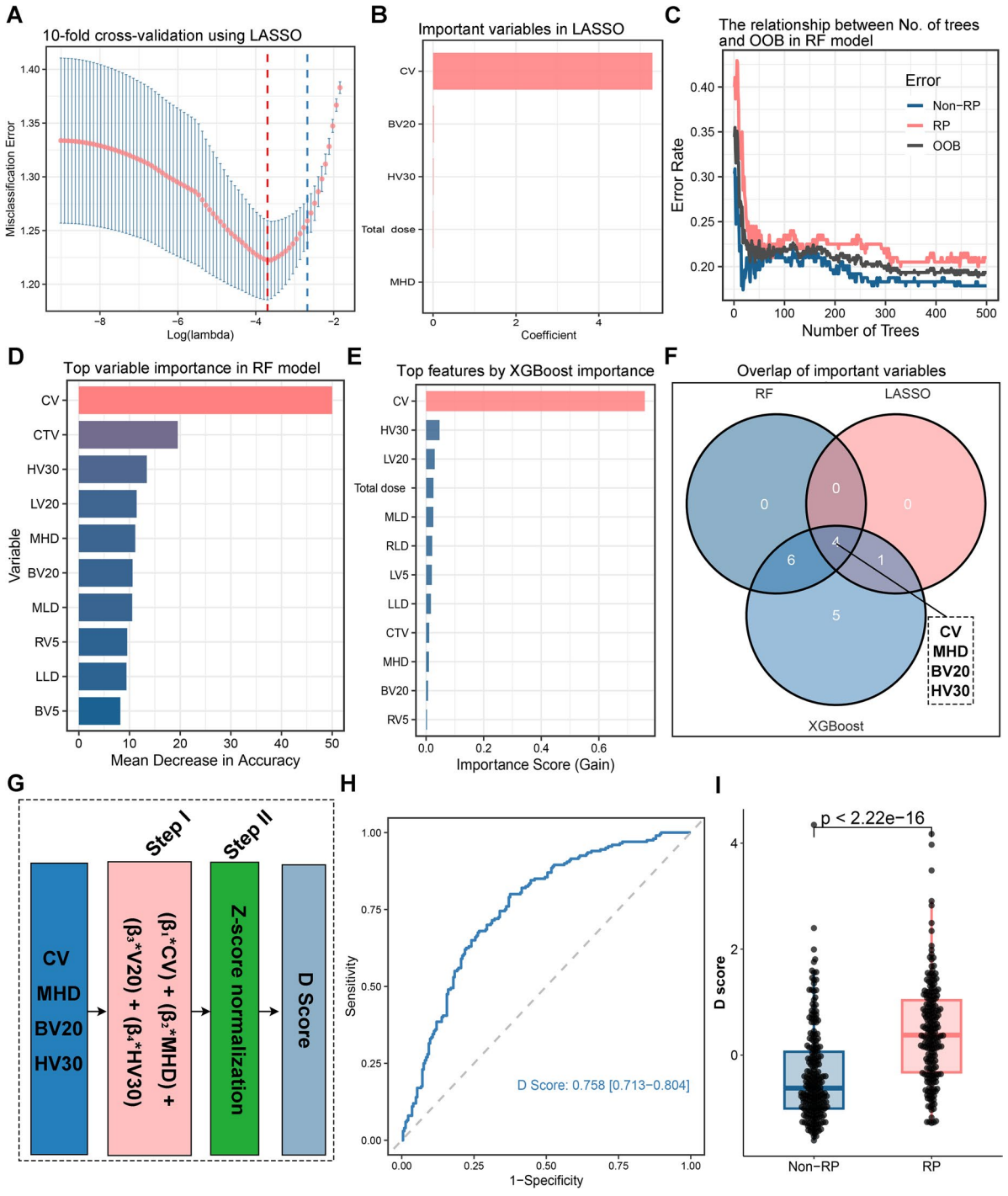

Figure 2. Machine learning-based screening of dosimetric parameters closely associated with the occurrence of RP at any grade and establishment of a dosimetric score. (A) The optimal lambda value was determined *via* 10-fold cross-validation in LASSO regression to assess the importance of dosimetric variables. (B) Key dosimetric variables were ranked based on regression coefficients. (C) The OOB error rate of the RF algorithm indicated stabilization of the dataset's error rate. (D) Dosimetric variables were ranked by importance using the RF algorithm. (E) The XGBoost algorithm was employed to identify significant dosimetric variables. (F) Venn diagram illustrating the four key dosimetric parameters identified by LASSO, RF, and XGBoost algorithms. (G) Logistic regression coefficients derived from the selected dosimetric variables were used to construct the composite *D* score, which was standardized using *Z* scores. (H) ROC curve of the *D* score model (AUC = 0.758, 95% CI: 0.713–0.804). (I) Box plot demonstrating significantly lower *D* scores in the non-RP group compared to the RP group ($p < 0.001$), with *p* values calculated using the Wilcoxon rank-sum test. BV5, percentage of both lungs volume receiving ≥5 Gy; BV20, percentage of both lungs volume receiving ≥20 Gy; CTV, clinical target volume; CV, clinical target volume to lung volume ratio; LV20,percentage of left lung volume receiving ≥20 Gy; MHD, mean heart dose; HV30, percentage of heart volume receiving ≥30 Gy; MLD, mean lung dose; Lasso, least absolute shrinkage and selection operator; LLD, left lung volume; OOB, out-of-bag; RF, random forest; RLD, right lung volume; RV5, percentage of right lung volume receiving ≥5 Gy; XGBoost, xtreme gradient boosting.

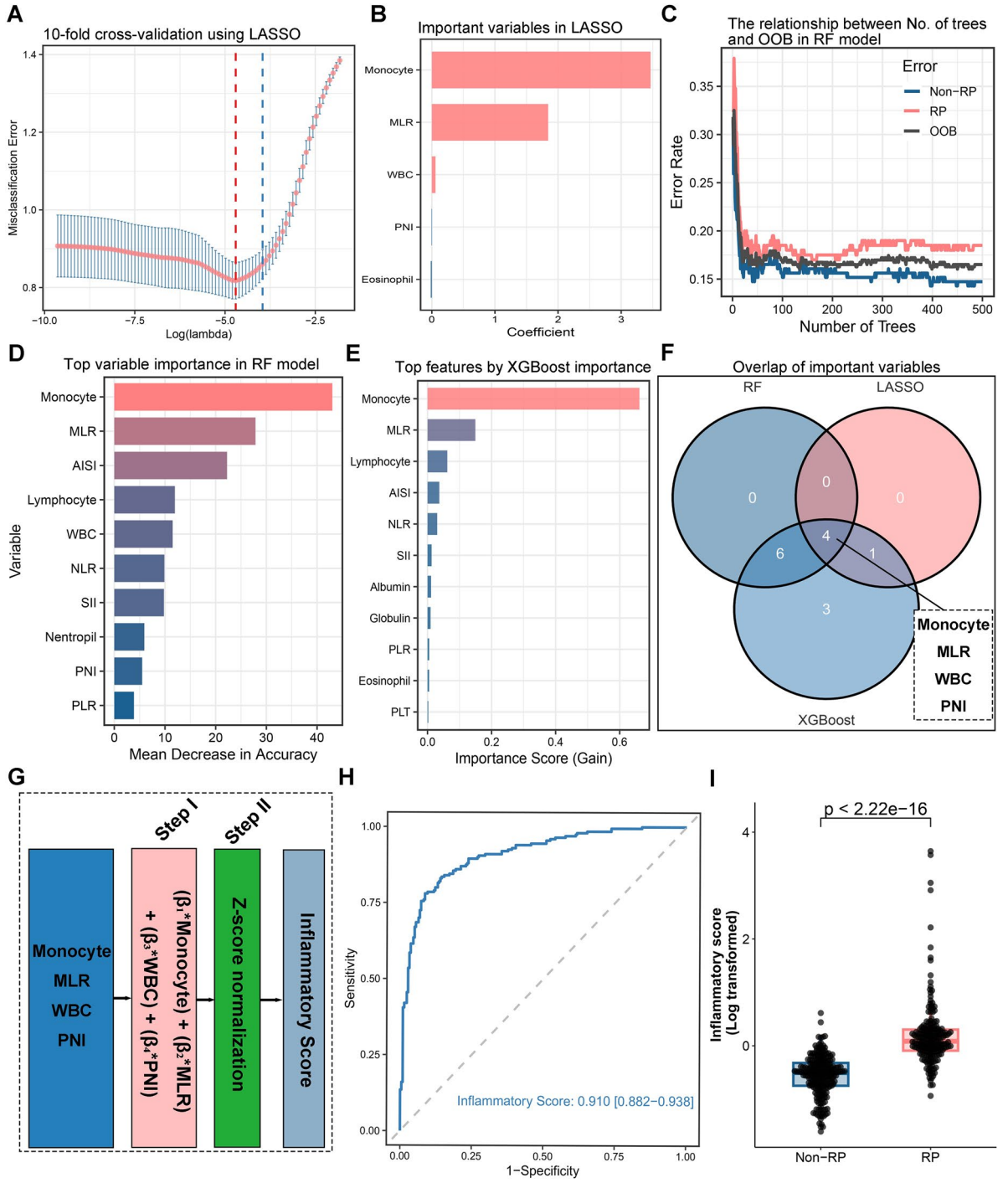

Figure 3. Machine learning-based screening of hematological parameters closely associated with the occurrence of RP at any grade and establishment of a hematological score. (A) The optimal lambda value was determined *via* 10-fold cross-validation in LASSO regression to assess the importance of hematological variables. (B) Key hematological variables were ranked based on regression coefficients. (C) The OOB error rate of the RF algorithm indicated stabilization of the dataset's error rate. (D) Hematological variables were ranked by importance using the RF algorithm. (E) The XGBoost algorithm was employed to identify significant hematological variables. (F) Venn diagram illustrating the four key hematological parameters identified by LASSO, RF, and XGBoost algorithms. (G) Logistic regression coefficients derived from the selected hematological variables were used to construct the composite *D* score, which was standardized using *Z* scores. (H) ROC curve of the *D* score model (AUC = 0.758, 95% CI: 0.713–0.804). (I) Box plot demonstrating significantly lower *D* scores in the non-RP group compared to the RP group ($p < 0.001$), with *p* values calculated using the Wilcoxon rank-sum test. AISI, aggregate index of systemic inflammation; Lasso, least absolute shrinkage and selection operator; MLR, monocyte to lymphocyte ratio; NLR, neutrophil to lymphocyte ratio; OOB, out-of-bag; RF, random forest; PLR, platelet to lymphocyte ratio; PNI, prognostic nutritional index; SII, systemic immune-inflammation index; WBC, white blood cell; XGBoost, xtreme gradient boosting.

Table 2. Univariate and multivariate logistic regression analysis of significant clinical variables and two models for predicting any-grade RP.

	Univariate		Multivariate	
Variables	OR (95%CI)	*P* value	OR (95%CI)	*P* value
Smoke score				
High				
Low	1.94 (1.32–2.86)	<0.001	1.61 (0.87–2.97)	0.131
PS				
0–1				
2	2.28 (1.53–3.40)	<0.001	1.65 (0.88–3.10)	0.121
CCI				
High				
Low	0.34 (0.16–0.75)	0.007	0.39 (0.12–1.24)	0.110
T2DM				
None				
Yes	7.31 (4.13–12.94)	<0.001	4.75 (2.21–10.18)	<0.001
ILD				
Probable UIP pattern				
Indeterminate and alternative diagnosis	0.57 (0.25–1.28)	0.174	0.51 (0.16–1.62)	0.251
UIP pattern	6.12 (2.99–12.54)	<0.001	5.49 (1.98–15.19)	0.001
Receive immunotherapy				
None				
Yes	4.92 (3.21–7.55)	<0.001	3.35 (1.76–6.35)	<0.001
ChemoRTregimen				
Sequential				
Concurrent	3.45 (2.22–5.26)	<0.001	2.27 (1.16–4.55)	0.017
Unknown	7.69 (2.38–25.00)	<0.001	1.85 (0.35–10.00)	0.466
Number of radiation sessions				
<28				
≥28	2.48 (1.67–3.67)	<0.001	1.59 (0.82–3.09)	0.170
Lung volume				
High				
Low	2.07 (1.40–3.05)	<0.001	2.41 (1.28–4.54)	0.007
D score				
High				
Low	0.18 (0.12–0.27)	<0.001	0.26 (0.14–0.50)	<0.001
Inflamm score				
High				
Low	0.03 (0.01–0.06)	<0.001	0.04 (0.02–0.09)	<0.001

CCI, Charlson comorbidity Index; ILD, interstitial lung disease; PS, performance status; RT, radiation therapy; T2DM, type 2 diabetes; UIP, usual interstitial pneumonia.

between predicted and observed RP risk (Figure 4C), and DCA showed greater net clinical benefit across a range of threshold probabilities (Figure 4D). Patients with RP had significantly higher nomogram-predicted score (Figure 4E). Subgroup analyses suggested superior performance of the integrated model in specific populations, such as patients younger than 65 years old and those with stage III–IV disease (Figure 4F–I).

Clinical application scenario

For clinical application, patients were dichotomized into high- and low-risk groups using the median (111) of the nomogram total points as the cut-off. Individuals with total points >111 were classified as high-risk and those with ≤111 as low-risk. Representative cases from each group (five per group) were reviewed to illustrate differences in clinical features, imaging findings, and outcomes (Figure 5; Supplementary Table 5). The high score group demonstrated more adverse clinical comorbidities, greater dosimetric exposure, and elevated systemic inflammation. All patients in the high-risk group developed RP during follow-up, with chest CT images revealing clear radiographic changes. In contrast, the low-risk group lacked such adverse factors; only rare cases of RP were observed and their CT findings remained largely stable. These observations support the integrated nomogram as a practical tool for individualized risk stratification and early identification of lung-cancer patients with pre-existing ILD who are at highest risk for RP, facilitating tailored treatment planning and follow-up. Future external multi-center validation studies are required to recalibrate the threshold according to different application scenarios, thereby obtaining clinical decision points that are better aligned with the practices of individual centers.

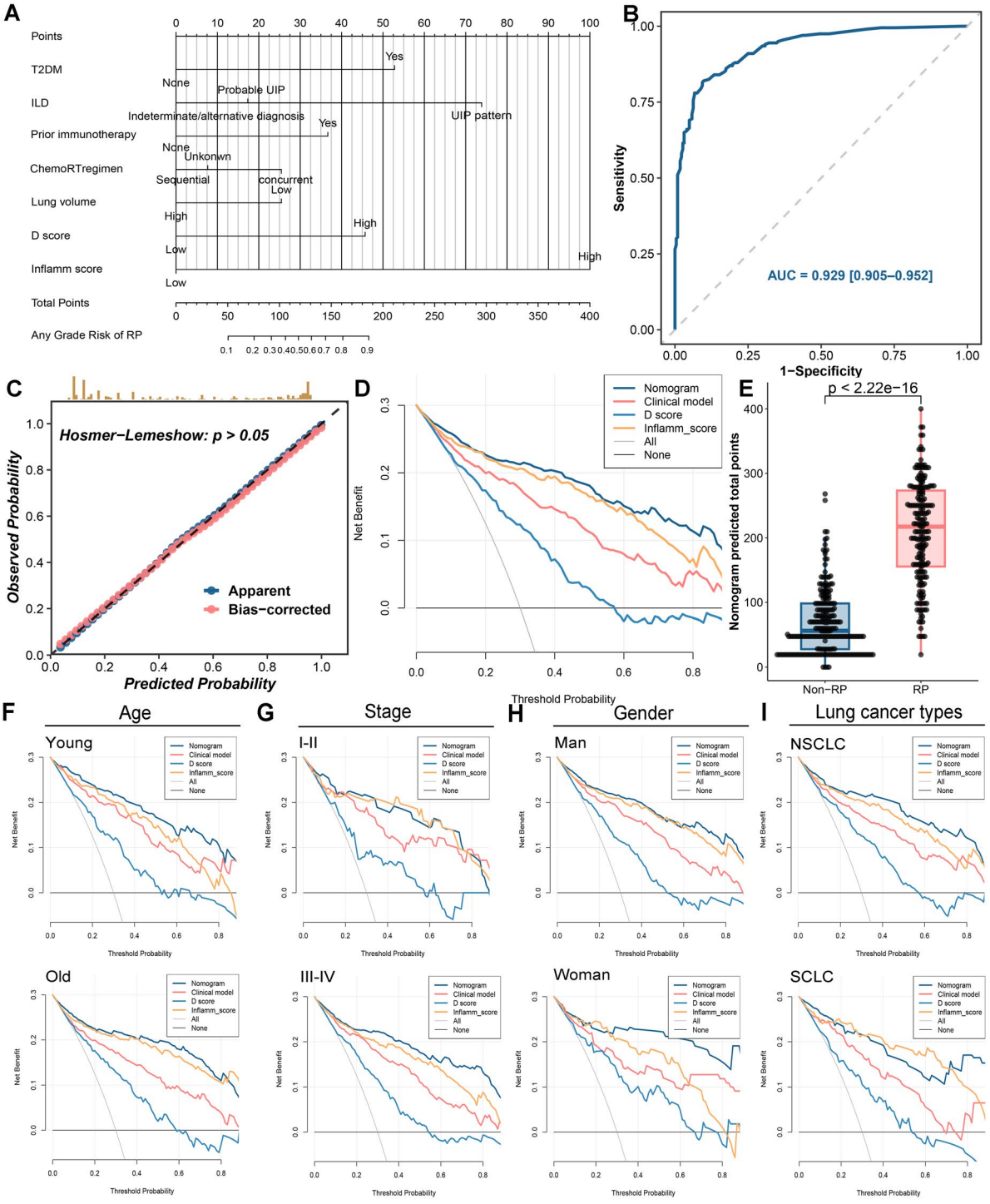

Figure 4. Development and evaluation of nomogram predictive model and assessment of the independent predictive performance of *D* score and Inflamm score. (A) Nomogram incorporating seven independent predictors to estimate the risk score for RP at any grade, providing individualized scores and stratifying patients into two prognostic groups. (B) ROC curve and (C) calibration curve of the nomogram model, with Hosmer–Lemeshow test results indicating good model fit ($P > 0.05$). (D) Decision curve analysis of different models, demonstrating superior net benefit of the nomogram model across various threshold probabilities. (E) Box plot showing significantly lower nomogram scores in the non-RP group compared to the RP group ($P < 0.001$). (F)–(I) Decision curve analyses for different subgroups: (F) Young (<65) and old (≥65) groups, (G) Stage I–II and III–IV groups, (H) Male and female groups, and (I) NSCLC and SCLC groups. ILD, interstitial lung disease; NSCLC, non-small cell lung cancer; ROC, receiver operating characteristic curve; SCLC, small cell lung cancer; T2DM, type 2 diabetes; UIP, usual interstitial pneumonia.

Table 3. DeLong's test for the four models.

Model	AUC	95% CI	*P* (vs Predict Prob)	*P* (vs Nomogram)
Basic clinical model	0.860	0.825–0.895	–	<0.001
Inflamm score	0.910	0.882–0.938	0.0204	0.168
D score	0.758	0.713–0.804	<0.001	<0.001
Nomogram	0.929	0.905–0.952	<0.001	–

AUC, area under the curve; CI, confidence interval.

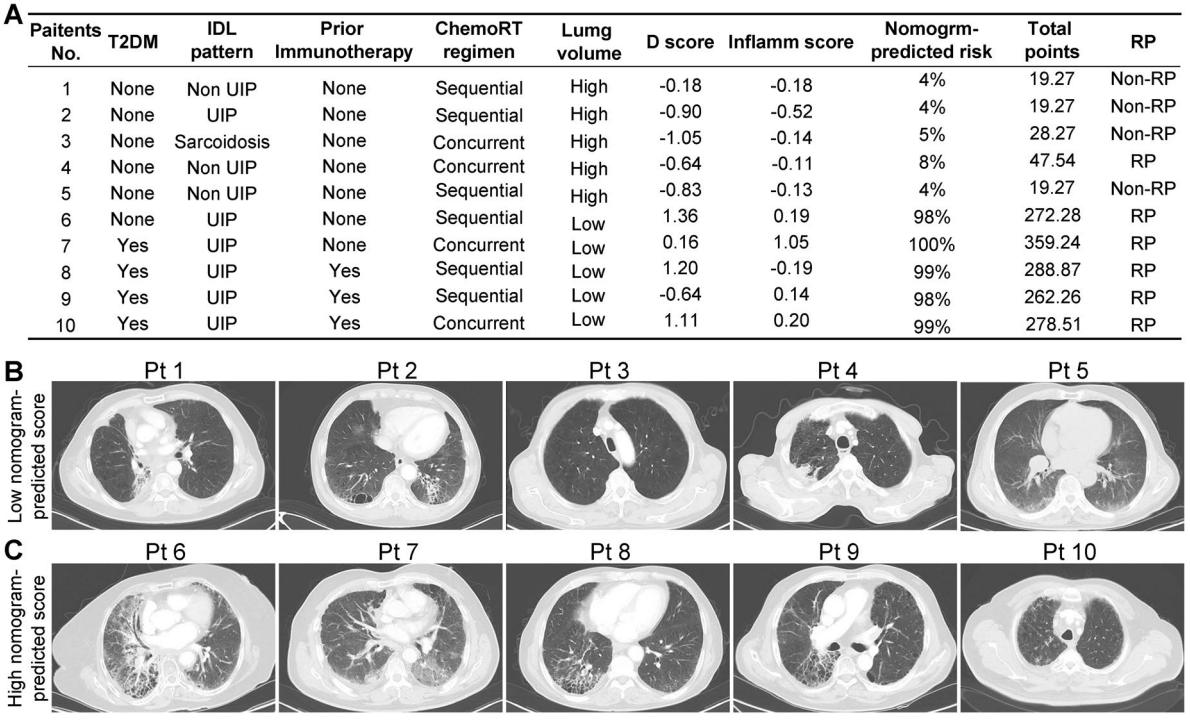

Figure 5. The clinical application scenario of the nomogram. (A) The nomogram-predicted score information for patients. (B) CT lung window images of representative patients with low nomogram-predicted score. (C) CT lung window images of representative patients with high nomogram-predicted score. CT, computed tomography.

Discussion

In this retrospective cohort of lung cancer patients with ILD undergoing thoracic radiotherapy, we developed a multivariable nomogram that integrates clinical characteristics, dosimetric metrics, and systemic inflammatory markers to estimate individual risk of RP. The nomogram demonstrated strong discrimination ability (AUC = 0.929) and outperformed single-domain comparators, including a dosimetry-only model (*D* score; AUC = 0.758) and an inflammation-only model (Inflamm score; AUC = 0.910). Notably, the Inflamm-score approached the performance of the full model and exceeded the *D* score, suggesting that, in patients with ILD, baseline systemic inflammation may carry more predicting information for RP than dose distribution alone. These findings support an integrated risk-assessment strategy that complements—rather than replaces—traditional dosimetric thresholds and may aid individualized treatment planning and surveillance.

Our findings suggest that the incidence of RP correlates with ILD severity, immunotherapy treatment, the specific radiochemotherapy regimen, coexisting T2DM, and reduced lung volume. Consistent with previous studies, ILD severity has been identified as a major risk factor for RP in this population [24,25]. The classification and severity of ILD are strongly associated with acute exacerbations, likely reflecting progressive parenchymal destruction during radiotherapy [26]. Immunotherapy was also confirmed as an independent risk factor for RP [27], possibly due to increased pulmonary radiosensitivity induced by immune checkpoint inhibitors [28]. Additionally, our study is the first to establish T2DM as an independent risk factor for RP in lung cancer patients with ILD, in line with prior findings in the general lung

cancer population [29,30]. This is likely because chronic hyperglycemia leads to increased secretion of inflammatory cytokines like IL-6 and higher production of reactive oxygen species by neutrophils [31,32], thereby augmenting the inflammatory response to radiation in diabetic patients [11]. Furthermore, our results corroborate previous reports that reduced lung volume is associated with higher RP risk [33]. Interestingly, we observed a higher risk of RP with concurrent chemoradiotherapy compared to sequential regimens, in contrast to some prior studies [34]. This discrepancy may be explained by differences in patient populations, as our cohort primarily consisted of patients with pre-existing ILD, who may be more susceptible to chemotherapy-induced toxicity [35].

While previous studies emphasized dosimetric predictors like MLD and Vx values [36–39], our findings challenge applying conventional dosimetric thresholds (e.g. V20 ≤ 30%, MLD ≤ 20 Gy) [35] to patients with ILD. A high RP incidence (47.2%) in our cohort, despite most meeting these criteria, underscores the inadequacy of dosimetric parameters alone. Although our dosimetric *D* score predicted RP, it was outperformed by the inflammatory score and the integrated nomogram. This aligns with recent findings that dosimetric factors are less predictive in patients with underlying lung disease [40].

The underlying mechanisms driving the heightened radiotoxicity in ILD patients remain poorly elucidated. These findings collectively suggest that the inflammatory response plays a pivotal role in the pathogenesis of RP. Further supporting these pathways, dysregulation of the TGF-β axis—particularly reduced TGFBR3—has been linked to pro-inflammatory and pro-fibrotic signaling in lung tissue, a biology that may heighten susceptibility to RP after thoracic irradiation [41]. In parallel, oxidative-stress–driven apoptosis and angiogenic signaling in lung-cancer models provide a mechanistic basis by which RT-induced ROS could synergize with baseline ILD-related inflammation to exacerbate alveolo-capillary injury [42]. These data are consistent with the superior predictive performance of the inflammation-based score observed in our cohort. Emerging evidence suggests that immune dysregulation, rather than classic local inflammation, may play a central role [43]. Corroborating this, our study demonstrates that hematological and inflammatory markers may be more critical predictors of RP development. This implies that the pathogenesis of RP in the ILD population may diverge from the traditional model, being more intricately linked to biological mechanisms like immune dysregulation and local inflammation. In ILD patients undergoing radiotherapy, radiation may not only inflict alveolar damage but also trigger aberrant immune responses, thus exacerbating RP development [44]. Our study uniquely identifies a high monocyte count as being closely associated with RP incidence. This may be related to increased C–C motif chemokine ligand 2 (CCL2) expression in the lungs of ILD patients [45], which is further induced by pulmonary radiation [46], leading to the massive recruitment of inflammatory monocytes that worsens lung injury [47], further underscoring the pivotal role of inflammatory activation in this cohort. Furthermore, consistent with the findings of Gao Y et al. our study confirmed a significant association between MLR and the development of RP [15]. More importantly, we are the first to identify a close correlation between PNI and RP. A plausible mechanistic link between PNI and RP can be framed along intertwined inflammatory and immune-competence pathways. Albumin, a negative acute-phase reactant, tracks systemic inflammation and nutritional reserve; lower albumin levels align with a pro-inflammatory state that facilitates the canonical cytokine network implicated in radiation-induced lung injury—particularly IL-1, IL-6, TNF-α, and TGF-β, which promote alveolar–capillary damage and fibro-proliferation [48]. Lymphocytes orchestrate early post-irradiation immune responses; radiation-induced lymphopenia perturbs T-cell–macrophage crosstalk and delays resolution of lung injury, a determinant of pneumonitis risk and outcomes after thoracic radiotherapy [49]. Taken together, these findings suggest that systemic inflammation—beyond localized cytokine production alone [50]—is central to RP in patients with ILD, underscoring the need for tailored risk-assessment strategies in this population.

To our knowledge, this is among the first large-sample studies to systematically compare clinical, dosimetric, and haematological predictors in ILD patients undergoing thoracic radiotherapy. Using multiple ML algorithms, we developed an integrated nomogram that showed excellent performance in predicting the risk of RP in this vulnerable population. This practical, user-friendly tool leverages routine pretreatment data to support individualized decision-making—optimizing treatment plans (e.g. minimizing the *D* score) and intensifying monitoring for patients with elevated inflammatory risk (high Inflamm-score).

Several limitations warrant consideration. First, the retrospective, single-centre design may introduce selection bias and limit generalizability. Second, despite rigorous machine-learning–based feature selection and cross-validation, external validation in independent, multicentre cohorts remains necessary to confirm robustness and transportability. Third, due to incomplete medical records, antifibrotic therapy was not included in the analysis in this study. However, recent studies suggest that antifibrotic drugs may mitigate radiation-induced lung injury [51]. Future prospective cohorts should standardize the documentation of antifibrotic drug exposure to verify its potential impact on the risk of radiation pneumonitis in high-risk UIP populations. Finally, although multi-omics approaches—including radiomics and genomics—have shown promise for predicting RP [52–54], such data were not included here. In future work, we will undertake multicentre external validation by aggregating clinical, dosimetric, and haematological data across institutions to evaluate the *D* score, Inflamm-score, and the final nomogram; integrate multi-omics by incorporating radiomics with Image Biomarker Standardization Initiative-compliant feature extraction, stability-driven feature selection, and ComBat harmonization [55], and by summarizing transcriptomic data as pathway activity scores; reassess model performance using nested, site-stratified cross-validation with calibration, clinical utility analysis, and SHapley Additive exPlanations (SHAP)-based interpretability [56,57] to support prospective deployment.

Conclusions

In summary, we developed an integrated predictive model combining clinical, dosimetric, and inflammatory parameters for individualized risk assessment of RP in lung cancer patients with pre-existing ILD undergoing radiotherapy. The proposed *D* score and Inflamm score, together with the constructed nomogram, provide practical tools for stratifying patients according to their risk and guiding personalized management strategies. These findings may facilitate more precise and proactive clinical decision-making for high-risk populations. Future multicenter prospective studies are needed to further validate these models and assess their impact in real-world clinical practice.

Acknowledgments

We gratefully acknowledge Shandong Cancer Hospital and Institute for providing access to its learning platform. We also thank the patients and their families for their invaluable contributions to this research.

Authors contributions

CRediT: **Haozheng Lu**: Conceptualization, Data curation, Formal analysis, Investigation, Methodology, Software, Writing – original draft, Writing – review & editing; **Aimin Jiang**: Conceptualization, Data curation, Formal analysis, Investigation, Methodology, Software, Writing – original draft, Writing – review & editing; **Zhaoqi Yuan**: Conceptualization, Data curation, Writing – review & editing; **Dawei Chen**: Funding acquisition, Supervision, Writing – review & editing.

Ethics approval

This study was complied with the Declaration of Helsinki and approved by the Ethics Committee of Shandong Cancer Hospital and Institute (approval number: SDTHEC 202501010). The need to obtain informed consent was waived by the Ethics Committee of the Shandong Cancer Hospital and Institute due to the retrospective nature of this study.

Disclosure statement

The authors declare that they have no known competing financial interests or personal relationships that could have appeared to influence the work reported in this paper.

Data sharing statement

Research data are stored in an institutional repository and will be shared upon request to the corresponding author.

Funding

This work was supported by the foundation of National Natural Science Foundation of China (82030082, 82172676, 82373217), the foundation of Natural Science Foundation of Shandong (ZR2023ZD26, ZR2024JQ032, ZR2021YQ52), Collaborative Academic Innovation Project of Shandong Cancer Hospital (GF001), Noncommunicable Chronic Diseases-National Science and Technology Major Project (2024ZD0519900, 2024ZD0519902), the China Postdoctoral Science Foundation under Grant Number 2025M782135, and Project SDCX-ZG-202502079 funded by Postdoctoral Innovation Program of Shandong Province.

ORCID

Dawei Chen http://orcid.org/0000-0002-6762-7997

References

[1] Dileto CL, Travis EL. Fibroblast radiosensitivity *in vitro* and lung fibrosis *in vivo*: comparison between a fibrosis-prone and fibrosis-resistant mouse strain. Radiat Res. 1996;146(1):61–67.
[2] Käsmann L, Dietrich A, Staab-Weijnitz CA, et al. Radiation-induced lung toxicity – cellular and molecular mechanisms of pathogenesis, management, and literature review. Radiat Oncol. 2020;15(1):214. doi: 10.1186/s13014-020-01654-9.
[3] Goodman CD, Nijman SFM, Senan S, et al. A primer on interstitial lung disease and thoracic radiation. J Thorac Oncol. 2020;15(6):902–913. doi: 10.1016/j.jtho.2020.02.005.
[4] Frank AJ, Dagogo-Jack I, Dobre IA, et al. Management of lung cancer in the patient with interstitial lung disease. Oncologist. 2023;28(1):12–22. doi: 10.1093/oncolo/oyac226.
[5] Jiang A, Lu H, Zhao R, et al. The impact of pre-existing interstitial lung disease on radiation and checkpoint inhibitor pneumonitis in lung cancer patients: a systematic review and meta-analysis. Ther Adv Med Oncol. 2025;17:17588359251338624. doi: 10.1177/17588359251338624.
[6] Okumura M, Hojo H, Nakamura M, et al. Radiation pneumonitis after palliative radiotherapy in cancer patients with interstitial lung disease. Radiother Oncol. 2021;161:47–54. doi: 10.1016/j.radonc.2021.05.026.
[7] Hou Z, Kong Y, Wu J, et al. A deep learning model for translating CT to ventilation imaging: analysis of accuracy and impact on functional avoidance radiotherapy planning. Jpn J Radiol. 2024;42(7):765–776. doi: 10.1007/s11604-024-01550-2.
[8] Cheng N, Chen C, Liu J, et al. DeepLCRmiRNA: a hybrid neural network approach for identifying lung cancer-associated miRNAs. Curr Gene Ther. 2025;25(4):559–565. doi: 10.2174/0115665232312364240902060458.
[9] Zhou L, Wen Y, Zhang G, et al. Machine learning-based multiomics prediction model for radiation pneumonitis. J Oncol. 2023;2023:5328927–5328929. doi: 10.1155/2023/5328927.
[10] Kang J, Coates JT, Strawderman RL, et al. Genomics models in radiotherapy: from mechanistic to machine learning. Med Phys. 2020;47(5):e203–e217. doi: 10.1002/mp.13751.
[11] Arroyo-Hernández M, Maldonado F, Lozano-Ruiz F, et al. Radiation-induced lung injury: current evidence. BMC Pulm Med. 2021;21(1):9. doi: 10.1186/s12890-020-01376-4.
[12] Haanen J, Obeid M, Spain L, et al. Management of toxicities from immunotherapy: ESMO Clinical Practice Guideline for diagnosis, treatment and follow-up. Ann Oncol. 2022;33(12):1217–1238. doi: 10.1016/j.annonc.2022.10.001.
[13] Freites-Martinez A, Santana N, Arias-Santiago S, et al. Using the Common Terminology Criteria for Adverse Events (CTCAE-Version 5.0) to evaluate the severity of adverse events of anticancer therapies. Actas Dermosifiliogr (Engl Ed). 2021;112(1):90–92. doi: 10.1016/j.ad.2019.05.009.
[14] Nishino M. Imaging of oncologic treatment-related pneumonitis: a focused review on emerging issues of immune checkpoint inhibitor pneumonitis, from the AJR special series on inflammation. AJR Am J Roentgenol. 2022;218(1):19–27. doi: 10.2214/ajr.21.25454.
[15] Gao Y, Wu X, Li Y, et al. The predictive value of MLR for radiation pneumonia during radiotherapy of thoracic tumor patients. Cancer Manag Res. 2020;12:8695–8701. doi: 10.2147/cmar.S268964.
[16] Lee DS. Clinical implications of the serum platelet-to-lymphocyte ratio in the modern radiation oncology era: research update and literature review. Radiat Oncol. 2024;19(1):107. doi: 10.1186/s13014-024-02485-8.
[17] Shan J, Xie X, Gu B, et al. Inflammation index predicts radiation-induced lung injury and prognosis in lung tumors treated with stereotactic body radiation therapy. Jpn J Radiol. 2024;42(1):102–108. doi: 10.1007/s11604-023-01482-3.
[18] Ma L, Ye W, Li Q, et al. Subjective global assessment (SGA) score could be a predictive factor for radiation pneumonitis in lung cancer patients with normal pulmonary function treated by intensity-modulated radiation therapy and concurrent chemotherapy. Clin Lung Cancer. 2018;19(2):e211–e217. doi: 10.1016/j.cllc.2017.09.001.

[19] Hatabu H, Hunninghake GM, Richeldi L, et al. Interstitial lung abnormalities detected incidentally on CT: a Position Paper from the Fleischner Society. Lancet Respir Med. 2020;8(7):726–737. doi: 10.1016/s2213-2600(20)30168-5.
[20] Washko GR, Lynch DA, Matsuoka S, et al. Identification of early interstitial lung disease in smokers from the COPDGene study. Acad Radiol. 2010;17(1):48–53. doi: 10.1016/j.acra.2009.07.016.
[21] Hata A, Schiebler ML, Lynch DA, et al. Interstitial lung abnormalities: state of the art. Radiology. 2021;301(1):19–34. doi: 10.1148/radiol.2021204367.
[22] Raghu G, Remy-Jardin M, Richeldi L, et al. Idiopathic pulmonary fibrosis (an update) and progressive pulmonary fibrosis in adults: an official ATS/ERS/JRS/ALAT clinical practice guideline. Am J Respir Crit Care Med. 2022;205(9):e18–e47. doi: 10.1164/rccm.202202-0399ST.
[23] Jaula H, Mattila L, Lappi-Blanco E, et al. Clinical, radiological and histopathological features of patients with familial pulmonary fibrosis. Respir Res. 2024;25(1):239. doi: 10.1186/s12931-024-02864-5.
[24] Ozawa Y, Abe T, Omae M, et al. Impact of preexisting interstitial lung disease on acute, extensive radiation pneumonitis: retrospective analysis of patients with lung cancer. PLoS One. 2015;10(10):e0140437. doi: 10.1371/journal.pone.0140437.
[25] Li F, Liu H, Wu H, et al. Risk factors for radiation pneumonitis in lung cancer patients with subclinical interstitial lung disease after thoracic radiation therapy. Radiat Oncol. 2021;16(1):70. doi: 10.1186/s13014-021-01798-2.
[26] Kobayashi H, Naito T, Omae K, et al. Impact of interstitial lung disease classification on the development of acute exacerbation of interstitial lung disease and prognosis in patients with stage III non-small-cell lung cancer and interstitial lung disease treated with chemoradiotherapy. J Cancer. 2018;9(11):2054–2060. doi: 10.7150/jca.24936.
[27] Kanai O, Kim YH, Demura Y, et al. Efficacy and safety of nivolumab in non-small cell lung cancer with preexisting interstitial lung disease. Thorac Cancer. 2018;9(7):847–855. doi: 10.1111/1759-7714.12759.
[28] Louvel G, Bahleda R, Ammari S, et al. Immunotherapy and pulmonary toxicities: can concomitant immune-checkpoint inhibitors with radiotherapy increase the risk of radiation pneumonitis? Eur Respir J. 2018;51(1):1701737. doi: 10.1183/13993003.01737-2017.
[29] Dong G, Li Y, Zhao Q, et al. Effects of diabetes on the development of radiation pneumonitis. Respir Res. 2021;22(1):160. doi: 10.1186/s12931-021-01754-4.
[30] Kong M, Lim YJ, Kim Y, et al. Diabetes mellitus is a predictive factor for radiation pneumonitis after thoracic radiotherapy in patients with lung cancer. Cancer Manag Res. 2019;11:7103–7110. doi: 10.2147/cmar.S210095.
[31] Malenica M, Šilar M, Dujić T, et al. Importance of inflammatory markers and IL-6 for diagnosis and follow up of patients with type 2 diabetes mellitus. Med Glas (Zenica). 2017;14(2):169–175. doi: 10.17392/920-17.
[32] Alexandraki KI, Piperi C, Ziakas PD, et al. Cytokine secretion in long-standing diabetes mellitus type 1 and 2: associations with low-grade systemic inflammation. J Clin Immunol. 2008;28(4):314–321. doi: 10.1007/s10875-007-9164-1.
[33] Briere TM, Krafft S, Liao Z, et al. Lung size and the risk of radiation pneumonitis. Int J Radiat Oncol Biol Phys. 2016;94(2):377–384. doi: 10.1016/j.ijrobp.2015.10.002.
[34] Vogelius IR, Bentzen SM. A literature-based meta-analysis of clinical risk factors for development of radiation induced pneumonitis. Acta Oncol. 2012;51(8):975–983. doi: 10.3109/0284186x.2012.718093.
[35] Ozawa Y, Koda K, Akahori D, et al. Preexisting interstitial lung disease and lung injury associated with irinotecan in patients with neoplasms. Anticancer Res. 2018;38(10):5937–5941. doi: 10.21873/anticanres.12939.
[36] Kim M, Lee J, Ha B, et al. Factors predicting radiation pneumonitis in locally advanced non-small cell lung cancer. Radiat Oncol J. 2011;29(3):181–190. doi: 10.3857/roj.2011.29.3.181.
[37] Madani I, De Ruyck K, Goeminne H, et al. Predicting risk of radiation-induced lung injury. J Thorac Oncol. 2007;2(9):864–874. doi: 10.1097/JTO.0b013e318145b2c6.
[38] Palma DA, Senan S, Tsujino K, et al. Predicting radiation pneumonitis after chemoradiation therapy for lung cancer: an international individual patient data meta-analysis. Int J Radiat Oncol Biol Phys. 2013;85(2):444–450. doi: 10.1016/j.ijrobp.2012.04.043.
[39] Rodrigues G, Lock M, D'Souza D, et al. Prediction of radiation pneumonitis by dose–volume histogram parameters in lung cancer: a systematic review. Radiother Oncol. 2004;71(2):127–138. doi: 10.1016/j.radonc.2004.02.015.
[40] Park SH, Lim JK, Kang MK, et al. Predictive factors for severe radiation-induced lung injury in patients with lung cancer and coexisting interstitial lung disease. Radiother Oncol. 2024;192:110053. doi: 10.1016/j.radonc.2023.110053.
[41] Deng X, Ma N, He J, et al. The role of TGFBR3 in the development of lung cancer. Protein Pept Lett. 2024;31(7):491–503. doi: 10.2174/0109298665315841240731060636.
[42] Ullah A, Razzaq A, Alfaifi MY, et al. Sanguinarine attenuates lung cancer progression via oxidative stress-induced cell apoptosis. Curr Mol Pharmacol. 2024;17:e18761429269383. doi: 10.2174/0118761429269383231119062233.
[43] Morgan GW, Breit SN. Radiation and the lung: a reevaluation of the mechanisms mediating pulmonary injury. Int J Radiat Oncol Biol Phys. 1995;31(2):361–369. doi: 10.1016/0360-3016(94)00477-3.
[44] Sakagami M, Inokuchi H, Mukumoto N, et al. Clinical features and risk factors for interstitial lung disease spreading in low-dose irradiated areas after definitive radiotherapy with or without durvalumab consolidation therapy for patients with non-small cell lung cancer. Radiat Oncol. 2023;18(1):87. doi: 10.1186/s13014-023-02276-7.
[45] Suga M, Iyonaga K, Ichiyasu H, et al. Clinical significance of MCP-1 levels in BALF and serum in patients with interstitial lung diseases. Eur Respir J. 1999;14(2):376–382. doi: 10.1034/j.1399-3003.1999.14b23.x.

[46] Cappuccini F, Eldh T, Bruder D, et al. New insights into the molecular pathology of radiation-induced pneumopathy. Radiother Oncol. 2011;101(1):86–92. doi: 10.1016/j.radonc.2011.05.064.
[47] Groves AM, Johnston CJ, Williams JP, et al. Role of infiltrating monocytes in the development of radiation-induced pulmonary fibrosis. Radiat Res. 2018;189(3):300–311. doi: 10.1667/rr14874.1.
[48] Lierova A, Jelicova M, Nemcova M, et al. Cytokines and radiation-induced pulmonary injuries. J Radiat Res. 2018;59(6):709–753. doi: 10.1093/jrr/rry067.
[49] Wang X, Wang P, Zhao Z, et al. A review of radiation-induced lymphopenia in patients with esophageal cancer: an immunological perspective for radiotherapy. Ther Adv Med Oncol. 2020;12:1758835920926822. doi: 10.1177/1758835920926822.
[50] Yan Y, Fu J, Kowalchuk RO, et al. Exploration of radiation-induced lung injury, from mechanism to treatment: a narrative review. Transl Lung Cancer Res. 2022;11(2):307–322. doi: 10.21037/tlcr-22-108.
[51] Zhang K, Ren L, Zhai Y. Effect and mechanism of Nintedanib on acute and chronic radiation-induced lung injury in mice. PLoS One. 2025;20(5):e0324339. doi: 10.1371/journal.pone.0324339.
[52] Zhang Z, Wang Z, Yan M, et al. Radiomics and dosiomics signature from whole lung predicts radiation pneumonitis: a model development study with prospective external validation and decision-curve analysis. Int J Radiat Oncol Biol Phys. 2023;115(3):746–758. doi: 10.1016/j.ijrobp.2022.08.047.
[53] Choi SH, Kim E, Heo SJ, et al. Integrative prediction model for radiation pneumonitis incorporating genetic and clinical–pathological factors using machine learning. Clin Transl Radiat Oncol. 2024;48:100819. doi: 10.1016/j.ctro.2024.100819.
[54] Yang S, Yao Y, Dong Y, et al. Prediction of radiation pneumonitis using genome-scale flux analysis of RNA-Seq derived from peripheral blood. Front Med (Lausanne). 2021;8:715961. doi: 10.3389/fmed.2021.715961.
[55] Leithner D, Nevin RB, Gibbs P, et al. ComBat harmonization for MRI radiomics: impact on nonbinary tissue classification by machine learning. Invest Radiol. 2023;58(9):697–701. doi: 10.1097/rli.0000000000000970.
[56] Vickers AJ, Elkin EB. Decision curve analysis: a novel method for evaluating prediction models. Med Decis Mak. 2006;26(6):565–574. doi: 10.1177/0272989x06295361.
[57] Lundberg SM, Erion G, Chen H, et al. From local explanations to global understanding with explainable AI for trees. Nat Mach Intell. 2020;2(1):56–67. doi: 10.1038/s42256-019-0138-9.